Aetheras - Deepening our knowledge of planetary system formation and evolution by studying atmospheric escape

Marius Anger, Aksel Søren Beltoft, Noria Brecher, Antoine Corne, Jo Ann Egger, Simone Filomeno, Margarida Graça, Viktoria Keusch, Guillem Khairy, Jakub Kowalczyk, Dominik F. Loidolt, Melker Marminge, Alex McDougall-Page, Lukas Tamulevicius and Elena Tonucci

ABSTRACT

Many of the exoplanets discovered to date do not have equivalents in the Solar systems, which means there are still many open questions concerning the compositions and atmospheres of these objects, as well as their formation and evolution. By investigating the atmospheric escape some of these objects undergo and measuring proxies of magnetic fields, Aetheras will investigate some of the key questions in the exoplanet field today, namely the origin of the radius valley, the hot Neptune desert, and whether the presence of a magnetic field in a planet enhances or prohibits atmospheric loss. This will be achieved by measuring proxies of both atmospheric escape and magnetic fields in the NIR (1082.60 – 1084.00) ± 0.05 nm and UV (121.40 – 281.00) ± 0.05 nm.

1. Introduction

To date, there are 5470 confirmed exoplanets. Each of these exoplanets has its own unique set of properties, such as radius, mass, core, atmospheric composition (if any), distance to the host star, and orbital period [1].

There are several methods to discover exoplanets, one of which is the transit method. With this method, a planet is detected as it passes between its host star and the observer, leading to the projected surface of the planet reducing the light flux received by the observer.

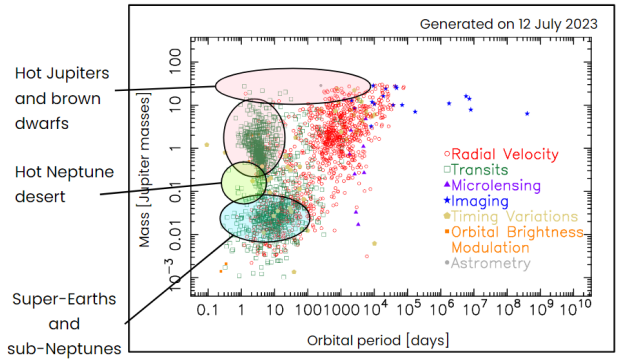

Figure 1: Distribution of the discovered exoplanets according to their orbital period and mass.

Among all the observed exoplanets, three types of commonly detected planets are not present in our Solar System, as shown in Figure 1:

- **Hot Jupiters**: gas giant exoplanets, with an orbital period of less than 10 days and closer than 0.1 AU from their host star.
- **Sub Neptunes**: planets with smaller radius than Neptune but near 2.0 R_E (earth radii).
- **Super Earths**: planets with bigger radius than Earth, yet lighter than ice giants.

Region 2 of Figure 1 includes both Hot Jupiters and Brown Dwarfs, the last of which are astrophysical bodies massive enough to fuse deuterium but not enough to fuse hydrogen ($13 < M < 80$ Jupiter masses). These bodies are expected to have magnetic fields due to their fast rotation period, there is also evidence suggesting atmospheric escape is taking place on Brown Dwarfs, as supported by observational evidence [2, 3, 4].

There is a noticeable gap in the number of planets found in region 3 of Figure 1. This gap is called the Hot Neptune desert and is defined by an absence of Neptune-size worlds that orbit close to their host stars. This less densely populated region cannot be explained by any known observational bias, which suggests some process is occurring, such as migration or atmospheric escape [5].

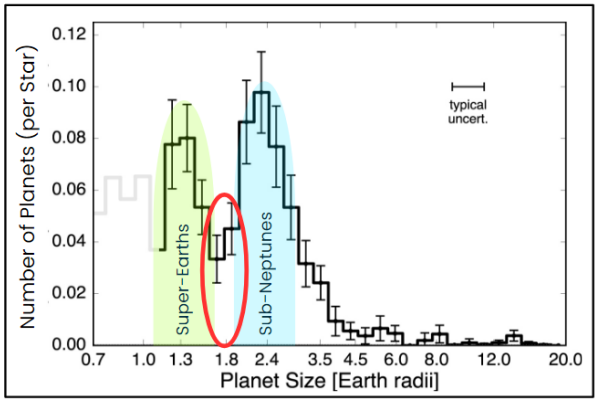

Figure 2: Number of planets per star according to their orbital period.

Similar to the hot Neptune desert, a gap is observed in the number of planets per star with a radius between 1.5 R_E and 2.0 R_E, as shown in Figure 2. This gap is called the radius valley.

The cause of both the radius valley and the Hot Neptune Desert is not yet understood and is highly debated. One hypothesis that is gaining traction is that the radius valley is an unstable region in which the planets are currently undergoing a transition towards a stable radius, instigated by atmospheric escape by, for example, photoevaporation [6], or core-powered mass loss [7], though several other processes have been suggested [8, 9]. It is believed that many features of the planets might influence the process and its rate, one of which might be the presence or lack of an intrinsic magnetic field [10]. Exoplanetary magnetospheres have yet to be unambiguously detected, yet is an active field of study as lately the common statement that a magnetosphere aids in retaining planetary atmospheres is being challenged. Traditionally, it is thought a magnetic field deflects the stellar wind that would ionise and drive away the atmosphere of the planet [11, 12]. The opposite hypothesis states that the presence of a magnetic field will increase the interaction area with the solar wind, leading to more frequent magnetic reconnection and thus enhancing ion upflow and cold plasma outflow [13].

2. Science

2.1. Science Questions and Objectives

The scientific theme of Aetheras is:

Deepening our knowledge of planetary system formation and evolution by studying atmospheric escape.

In accordance to this mission statement, Aetheras aims to answer the following scientific objectives:

SO1: Are there correlations between the characteristics of exoplanets, the properties of their host stars, and atmospheric escape?

SO2: Is atmospheric escape a factor in creating the radius valley?

SO3: Is atmospheric escape a factor in creating the hot Neptune desert?

SO4: How does the magnetic field of exoplanets influence atmospheric escape?

2.2. Measurement Methods

2.2.1. Atmospheric Escape Detection

Atmospheric escape can be detected through transmission spectroscopy during the transit of the planet. A planetary exosphere escaping from the planet can extend over many planetary radii, producing a comet-like tail, as shown in Figure 3. The particles in the tail are accelerated by radiation pressure and interactions with the stellar wind [14]. The presence of the tail affects the absorption of the star-light during the planetary transit. Looking at the light curves, an eventual in-transit excess absorption could indicate the presence of an escaping exosphere. Usually the transit depth varies from less than 1 % to 56 % (for a Neptune-mass planet) [15] indicating the presence of an outflow.

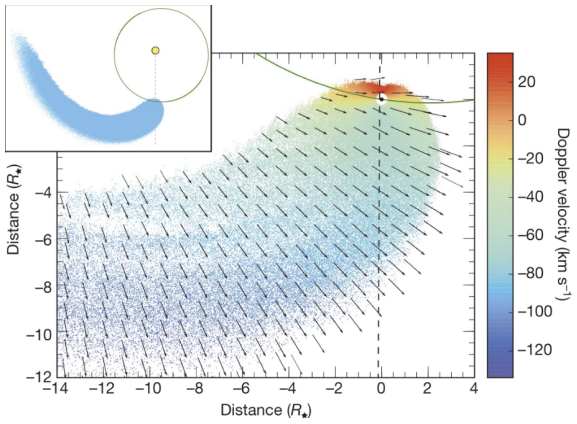

Figure 3: Three-dimensional simulation of the outflow tail coplanar with the line of sight. Arrows represent the hydrogen atom velocity and direction in the rest frame of the star. The outflow particles are colour-coded as a function of their projected velocities on the line of sight (dashed line). On the upper left of the image there is the full spatial extent of the exospheric cloud (in blue) on the orbital plane of the planet. [15]

The main proxies for atmospheric escape are the hydrogen Ly-α line (121.6 nm), the He I triplet metastable state transition line (1083 nm), and heavier species, like C II (133.45 nm), whose atmospheric escape in their exospheres happens hydrodynamically [16].

The standard spectroscopic channel to probe atomic H in exoplanet atmospheres is the Ly-α. The study of this line consists in performing a time-series observation of the Ly-α line of the host star before, during, and after the planetary transit as shown in Figure 4. The line is heavily affected by interstellar medium (ISM) absorption, so it can only be studied by observing its wings where the flux is significantly attenuated Figure 4. Interacting with the tail, the exospheric Ly-α signatures usually display asymmetries when compared to a traditional transit light curve at longer wavelengths.

A typical exospheric signal is a reduction in flux in the stellar Ly-α line during the planetary transit, which may be accompanied by both an extended egress and pre-transit absorption. This flux fluctuation is more noticeable in the blue wing because of the outflow direction (see Figure 3).

Like the Ly-α, the He triplet is a recent reliable technique to estimate atmospheric escape rates and study planetary outflows. Since it is a metastable state, it has a lifetime of 2.2 h, hence it is a promising origin of absorption lines. [17] Measuring the He I line spectrum during the transit, it is possible to observe how the absorption changes due to the excess absorption produced by the He atoms escaping the planetary atmosphere, the same way it happens for the Ly-α (see Figure 5). The information on the He I metastable line

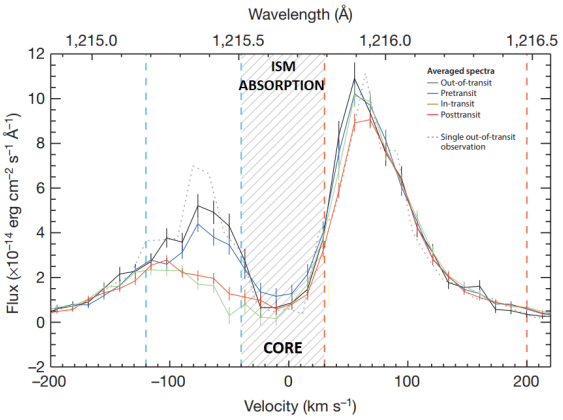

Figure 4: Evolution of the hydrogen Ly-α emission line of GJ 436. The line has been averaged over out-of-transit (black), pre-transit (blue), in-transit (green), and post-transit (red) observations from individual spectra. The hatched region (line core) cannot be observed from Earth because of the interstellar medium (ISM) absorption along the line of sight. [15]

is complementary to that obtained in the extended wings of the Ly-α line since they investigate different regions of the outflow. Moreover, this line can help constrain theoretical models of escaping exoplanet atmospheres [17].

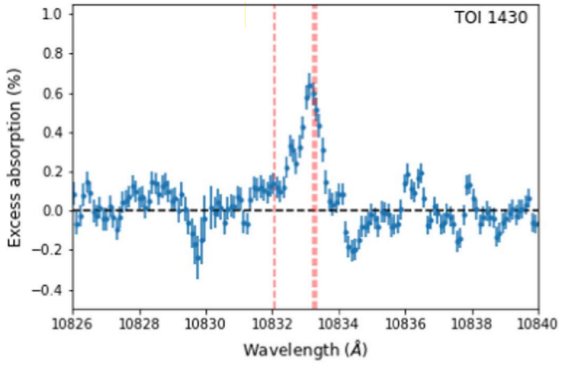

Figure 5: Average in-transit excess absorption spectrum of the HeI line for the transiting planet hosted by the TOI-1430 star. [18]

The transit spectroscopy technique used in Ly-α can be applied for metals, with the advantage that they have a highly reduced to absent ISM absorption [16]. These lines are much weaker and narrower than Ly-α, limiting the precision with which transit depths and outflow velocities can be measured. For this reason, the most studied line is the most intense line of C II.

The advantage of studying different lines from light elements (H, He I) to heavier metals (e.g., C II) is the improvement in the comprehension of how the atmospheric escaping processes work.

Extending the studied spectral range around the Ly-α and He I line, it is possible to study many different lines of interest for the scientific purposes in this mission, like N I 119.9 nm, Si I 124 nm, H_2O 128 nm, O I 130.4 nm, Si III 150 nm, C III 155 nm, Al I 169 nm, Na II 280.9 nm, K I 1102 nm lines.

2.2.2. *Magnetic Fields and Bow Shock Detection*

In addition to the characterisation of the atmospheric escape, the ionised metal species can be sensitive to planetary magnetic fields, forming controlled outflows and producing asymmetric transits if the field is strong enough. Even for this process, the C II line is the most used line which is studied by observing flux variation and asymmetries during the planetary transit.

An interesting phenomenon that can be used as a proxy for the presence of the magnetic field is the bow shock, which occurs when the stellar wind interacts with the magnetosphere of a planet, due to a sudden decrease in speed of the stellar wind particles. If the relative motion between the objects and stellar coronal material is supersonic, then the bow shock forms in the direction of motion. If the optical depth of the shocked material is high enough then starlight will be absorbed and produce an early ingress in the transit light curve as can be seen in Figure 6. Even if transit asymmetries for escaping metals are a matter of debate in the literature, early results pointed out the presence of a magnetospheric bow shock around WASP-12 b [19]. However, additional observations ruled out a stable early ingress [20], and the possibility of a variable bow shock remains open [16].

Another effect of the stellar wind and the magnetic field can be found in the velocity components by measuring the Doppler shift in the spectrum of the surrounding cloud [21].

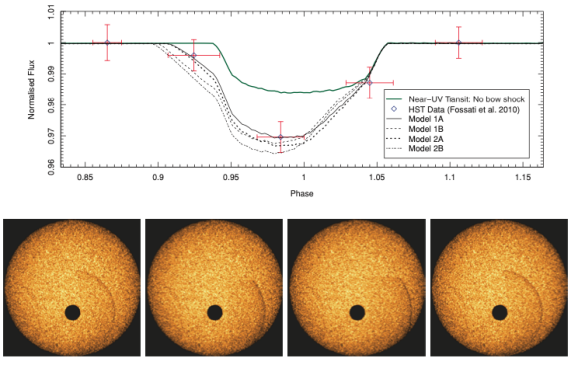

Figure 6: The top panel shows the modeled transits round WASP-12 b [near-UV: no bow shock (green), UV (black)] with the HST observations in red. The black lines represent the results of simulations. The bottom panel shows simulated mid-transit images. [19]

2.2.3. *Observation Expectations*

To solidify the scientific case, simulations of the expected signals were made to estimate the limits on the noise for the different bands. The flux contrast of the different lines was based on previous measurements of super-Earths. One of these simulations is found in Figure 7.

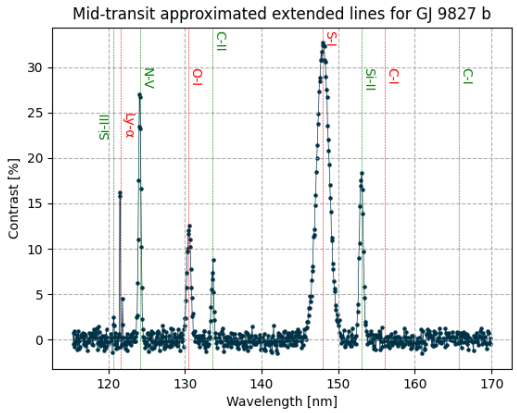

Figure 7: A simulation of expected flux contrast in % based on previous observations and with noise generated by NASAs Planetary Spectrum Generator.

2.3. Targets

A target list of exoplanets to be observed by the mission has been created. The targets were selected based on their fulfillment of the scientific objectives, their distance, absolute magnitude, and orbital period.
Specifically, 120 exoplanets in and around the radius valley have been selected along with 30 brown dwarfs, 100 hot Jupiters, and 50 hot Neptunes. A map of the target exoplanets' position on the projection of the celestial sphere is shown in the following Figure 8.

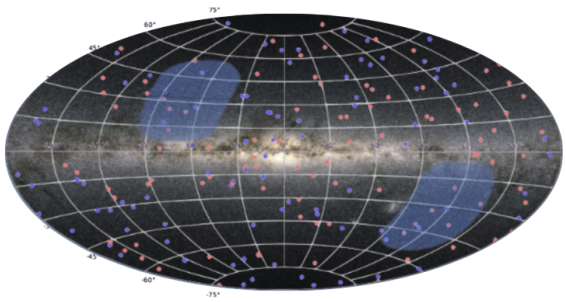

Figure 8: Image of the celestial sphere in a Galactic coordinate reference system. Targeted exoplanets are marked as red (radius valley) and purple (hot Neptunes, hot Jupiters, brown dwarfs,) dots. Additionally, the two provisional long-duration fields proposed by the space telescope PLATO are indicated in blue [22].

Furthermore, current and future missions are expected to confirm additional target exoplanets. Among these, the PLATO space telescope scheduled for launch in 2026 is expected to find an estimated 450-8000 radius valley targets, and 6000-20000 hot Jupiters. [22].

2.4. Current and Future missions

Several space missions including Hubble Space Telescope (HST), James Webb Space Telescope (JWST) and the future the Atmospheric Remote-sensing Infrared Exoplanet Large-survey (Ariel) can be used to characterize exoplanet atmospheres. The JWST's NIRSpec has a 0.6 µm to 5.0 µm wavelength range that can be used to study the He I emission line. But, the mission's substantial time requirement of at least 12000 hours renders it impractical for proposal. Furthermore, JWST lacks an UV spectrometer, which would constrain the scope and depth of the findings when compared to the outcomes achievable through a dedicated mission. Scheduled for launch in 2029, the ARIEL mission will conduct atmospheric characterisation of about 1000 transiting exoplanets using transit spectroscopy, spanning the wavelength range from 1.95 µm to 7.8 µm [23].
Nevertheless, Ariel lacks a UV spectrometer capable of detecting the Ly-α line and other specific UV emission lines that could indicate atmospheric loss or the presence of a magnetosphere. Furthermore, the low resolution in the near-IR (R>10) and mid-IR (R=30-200) of the AIRS does not resolve the He I line and thus won't allow detection of the rate of atmospheric escape. Ly-α observations can be obtained only by the HST as it is the only space observatory equipped with UV instruments (COS/STIS). The data obtained from these instruments present substantial challenges when it comes to interpretation.[24]. For instance, complexities can arise for Ly-α observations due to interstellar absorption and Earth geocoronal emission contamination [25]. In addition, the observations obtained from HST are subject to limitations caused by Earth occultations, consequently restricting the precision of measurements [16]. Finally, the inherently limited sensitivity of the instruments can result in a substantial number of planets remaining undetectable [14]. The unique integration of UV and IR spectrometers in the proposed mission has never been proposed to study exoplanets. This remarkable combination is expected to offer novel insights into the mechanism of atmospheric evolution of exoplanets and shed light on the coevolution of their atmospheres and magnetospheres.

2.5. Science Requirements

In order to answer the scientific questions posed in subsection 2.1, the following science requirements [SR] shall be fulfilled:

SR1. The mission shall measure proxies for atmospheric escape and magnetic fields in the NIR and UV, including the absorption lines:

- H Ly-α $(121.40 - 121.75) \pm 0.05$ nm
- C II $(130.00 - 137.00) \pm 0.05$ nm
- Mg II $(277.00 - 281.00) \pm 0.05$ nm
- He I $(1082.60 - 1084.00) \pm 0.05$ nm

[SO1, SO2, SO3, SO4]

This requirement follows from the previously explained measurement methods. In studying the formation of planetary systems through atmospheric escape mechanisms, the

given spectral lines can indicate the escaped particle tail (H Ly-α, Mg II, He I, C II), as well as magnetic bow shock (Mg II and C II).

In order to further study a possible correlation between an exoplanet's radius and its atmospheric properties, exoplanets from the following target groups are observed:

SR2. The mission shall observe at least 100 transiting exoplanets that lie in the radius valley or on its edges (1.2<R<2.3 R_E) using spectroscopy. [SO1, SO2, SO4]

SR3. The mission shall observe at least 100 transiting objects with a mass of at least 0.1 Jupiter masses. [SO1, SO4]

SR4. The mission shall observe at least 25 transiting Neptune-sised exoplanets with orbital periods of less than 4 days. [SO1, SO3, SO4]

SR5. The mission shall observe a minimum of 4 full transits per target, including ingress and egress, with a 2 h margin before and 50% transit duration margin after, acquiring at least 40 equidistant measurements per transit. [SO1, SO2, SO3, SO4]

The observation of the host star prior to the transit is crucial to observe a reference spectrum to the following transit. Additionally, as the bow shock is located in front of the planet, its effects would be measurable within the two hours interval before the transit. As the atmospheric escape is modeled as an outflow of particles, this particle tail would be measured during and after the transit duration.

SR6. The spectral resolution in the NIR shall be sufficient to measure a Doppler shift of at least 85 km/s in the He I absorption line. [SO1, SO2, SO3, SO4]

SR7. The spectral resolution in the UV shall be able to at least separate the Si III absorption line from the Ly-α absorption line. [SO1, SO2, SO3, SO4]

3. Instruments

3.1. Instrument Requirements

To ensure that the Science Requirements are met, Instrument Requirements [IR] have to be defined for the spacecraft and measurement instruments. These can be found in Table 1.
Additional absorption lines, such as those of H_2O, O, O_3, Si-I, or Si-III may also be observed, as those lie within the wavelengths covered by the IR instrument.

3.2. Optics

The mission features two spectrometers able to resolve the NIR and UV spectral ranges. The optical layout can be seen in Figure 9, and its related parameters in Table 2.
The light is collected by a Cassegrain telescope with a narrow angular field of view of 3.14° and a diameter of 1.5 m [M1]. The secondary mirror is integrated with a tip-tilt actuator to reduce the jitter of the point source on the detector at the end of the optical path. An additional visible (VIS) imaging channel is required to provide a steering signal for the tip-tilt mirror [TTM/M2] for fine target acquisition. A collimator [COLL1] brings the beam size down to 2 cm.
The first dichroic mirror [DICH1] is filtering UV light by spatial separation at a cut-off frequency of 300 nm to supply the UV instrument. The remaining frequencies are split into the VIS channel and the NIR channel by a second dichroic mirror [DICH2] with a cut-off frequency of 950 nm.

Table 1
Instrument Requirements [IR]

IR1.	The spacecraft shall be equipped with a spectrometer to perform simultaneous observations in the NIR $(1082.60 - 1084.00) \pm 0.05$ nm and UV $(121.40 - 281.00) \pm 0.05$ nm. [SR1]
IR2.	The photometric aperture shall capture 99.5% of the stellar flux in the NIR and the UV. [SR2, SR3, SR4, SR5]
IR3.	The resolving power shall be at least 3600 for the NIR. [SR6]
IR4.	The resolving power shall be at least 500 for the UV. [SR7]
IR5.	The photometric stability shall be better than 50 ppm (1σ) for the NIR instrument. [SR2, SR3, SR4, SR5]
IR6.	The photometric stability shall be better than 1% (1σ) for the UV. [SR2, SR3, SR4, SR5]
IR7.	The signal-to-noise ratio of the transition contrast shall be at least 8 for NIR. [SR2, SR3, SR4, SR5]
IR8.	The signal-to-noise ratio of the transition contrast shall be at least 4 for UV. [SR2, SR3, SR4, SR5]
IR9.	The instrument boresight shall not be pointed within a 15° cone towards Sun during operations. [SR2, SR3, SR4, SR5]
IR10.	The instrument shall be pointed with a pointing accuracy of 0.007 arcsec with a stability of 5% over at least 10 h towards the targets. [SR2, SR3, SR4, SR5]

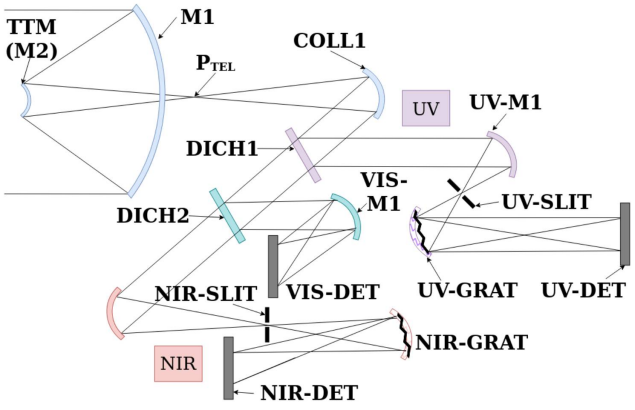

Figure 9: Optical layout of the UV, NIR, and VIS instrument

Table 2
Telescope and instrument parameters

M1	1.5 m
Angular FOV	3.14°
NIR Channel	1070 nm to 1090 nm
	Throughput: 34.78 %
	Spectral Resolution: 3724
UV Channel	115 nm to 285 nm
	Throughput: 1.75 %
	Spectral Resolution: 571
Compressed Data Rate	13.2 GB/day

In each spectrometer, a focusing mirror [UV-M1, NIR-M1] is used to adjust the focal stop ($F/24.4$) of the telescope to the needed focal stop of the respective instrument. This mirror is also used to focus the light through a slit [UV-SLIT, NIR-SLIT]. This is needed to restrict the light beam to the selected target star onto a concave blazed holographic diffraction grating [UV-GRAT, NIR-GRAT], which allows a shorter optical path and fewer optical elements and thus increasing the throughput of the system. In the focus of the diffraction grating a CCD [UV-DET, NIR-DET] is used to count the collected photons. The VIS channel only uses a single focusing lens [VIS-M1] to confine the light beam onto the target acquisition sensor. The presented optical system allows a maximum throughput of 1.94 % in the UV and 38.65 % in the NIR channel before splitting it into spectral bins.

3.3. UV Detector
The spacecraft is equipped with an ultraviolet (UV) detector featuring a pixel matrix of dimensions 1143x55, with each pixel measuring 4 microns and having an 8-bit depth. To ensure its accuracy, the detector is thermally stabilized. It generates approximately 0.5028571429 Mb of data per observation, offering crucial insights into the UV.

3.4. NIR Detector
The spacecraft incorporates a near-infrared (NIR) detector, featuring a matrix of 7448 by 49 pixels, with each pixel measuring 10 microns and having a depth of 16 bits. The NIR spectrum's higher flux compared to UV allows for higher resolution. The NIR detector requires careful cooling to minimize noise interference. The average data output from this detector is approximately 5.839448276 Mb.

3.5. VIS Detector
For accurate and stable positioning of the target onto the respective detector slit a feedback loop between the VIS channel detector and the tip-tilt mirror has to be used. The image of the target stars is continuously compared to the projected dot positions on both instruments to minimize the point spread function jitter on the respective spectrometer.

Table 3
Mission Requirements [MR]

MR1.	The mission shall be conducted at least 38 Earth radii away from Earth to be outside Earth's exosphere. [IR1, IR2, IR8, IR9, IR10]
MR2.	The mission shall provide a total scientific observation time of at least 12.000 hours. [SR2, SR4]
MR3.	The mission shall first observe the primary targets and afterwards observe the secondary targets. [SR2]

Table 4
Mission Constraints [MC]

MC1.	The mission shall use an Ariane 62 launcher for the space segment.
MC2.	The mission shall use a ground segment accessible by ESA.
MC3.	At the end of the lifetime, the mission shall be decommissioned by entering a graveyard orbit.

4. Mission Analysis

4.1. Orbit and Maneuvers
For orbit, the Lagrange point L2 has been chosen similar to JWST L2 is located behind the Earth viewed from the Sun. This choice is made due to a Ly-α image of the Earth taken from 0.1 AU with Hubble. This image showed that the geocorona extends more than 38 R_E (Kameda et al. 2017). The spacecraft will not need to orbit around the Earth, which would cause heating and cooling as it would orbit in and out of the Earth's shadow. At L2, the radiated heat from Earth is significantly less, providing a more stable viewpoint.

4.2. Mission Requirement
The Mission Requirements are detailed in Table 3. Key drivers of mission requirements include the need for a cost-efficient and safe orbit, far from the Earth's IR emission while remaining in constant Sun exposure. These requirements allow sufficient conditions to observe the whole range of aimed targets. To these requirements add the Mission Constraints, detailed in Table 4. To keep this mission inside the European scope, launchers were selected from the range offered by ESA.

4.3. Launcher selection
As stated above, the choice of launcher has been limited to Vega-C, Ariane 62, and Ariane 64. Considering the location of L2 and the mass of the spacecraft (see section 5), Ariane 62 was finally chosen.

4.4. Mission phases
The spacecraft will depart from Kourou (French Guyana), boarding Ariane 62. After a 30-minute burn toward L2, the satellite will detach from its launcher and deploy.
The transfer to L2 will last 60 days; followed by an estimated correction of 50 m/s before starting its commissioning. The

Table 5
System Requirements [SReq]

SReq1.	The spacecraft shall be 3-axis stabilised. [IR5, IR6, IR7, IR8]
SReq2.	The spacecraft shall have a propulsion system to perform orbit insertion, station keeping for at least 3 years, and disposal. [MR1, MC3]
SReq3.	The spacecraft shall withstand the radiation environment at the target orbit for at least 3 years. [MR1]
SReq4.	The spacecraft shall be able to observe targets between [-70°, 80°] in declination with respect to the ecliptic. [SR2, SR3, SR4]
SReq5.	The spacecraft shall fit in the payload module of the launcher. [MC1]
SReq6.	The spacecraft shall shield the instruments from straylight. [IR9]
SReq7.	The spacecraft shall be able to store at least 26.4Gb of data for at least 2 days. [IR3, IR4, IR5, IR6, IR7, IR8]
SReq8.	The spacecraft shall provide the necessary power for all operational modes. [MR2, MR3]
SReq9.	The spacecraft shall provide a cooling system for the NIR for at least lower than 140 K and the UV detector. [IR9, IR10, IR11, IR12]

observation phase is set to last 3 years. During this lifetime, station keeping will include orbit and attitude maintenance. After the observation phase, the spacecraft will be decommissioned into an unstable outbound orbit, far from Earth.

5. Spacecraft design

5.1. System Requirements

There are nine top-level system requirements identified which dictate the composition and engineering of the subsystems. These can be found in Table 5.

5.2. Attitude and Orbit Determination and Control System [AODCS]

With the mission performing precise measurements of targets tens of parsecs away, the AODCS needs to orient the spacecraft with 0.07" precision for measurement periods >10 hours. Additionally, the spacecraft shall have coarse pointing of >0.5°. A precision of 0.1 degrees is required for communication. The spacecraft shall be 3-axis stabilized, with a slewing rate over 0.05 deg/s and a momentum storage equal to 6.78 Nms. The spacecraft shall be able to perform launch error correction, yearly orbit maintenance, end-of-life decommissioning, and momentum dumping. The total Δv budget is included in Table 6. The spacecraft shall perform any of the orbit maneuvers within 300 s.

To meet these requirements, the spacecraft employs 2 star trackers to allow fine instrument pointing, as well as 6 Sun trackers for coarse pointing. As mentioned in section 3, the telescope's imager shall provide the needed precision for fine-pointing mode. 3 reaction wheels are used for attitude control, with a fourth included for redundancy. A single

Table 6
Δv budget

OPERATION	Δv requirement
Orbit Maintenance	1 m/s/yr
Launch Error	20 m/s
Decommissioning	50 m/s
Desaturation	2 m/s/yr

hydrazine 100 N main engine is included for orbital maneuvers and 20 hydrazine 1 N thrusters are used for momentum dumping and attitude control. This setup provides redundancy and keeps the exhausts as far from the telescope's axis as possible. All of the thrusters are hot gas variants with an I_{sp} of 220 s for 1 N and 190 s for the 100 N thruster.

The mass of all thrusters is 106 kg. The fuel shall be stored in one spherical tank with a mass of 13.5 kg. The reaction wheels shall have a combined mass of 20 kg. The total weight of the AODCS system shall be 185 kg with 20% margins. The weight of the fuel shall be 86.45 kg including 100% margin.

5.3. On-Board Data Handling [OBDH]

The OBDH will transfer and store payload, telemetry, and subsystem data between the different instruments. The OBDH data bus will be ESA standard, either MIL-STD-1553 or UART. The system will compress the produced scientific and telemetry data by 50 %, reducing the expected scientific data to 13.2 Gb/day. Due to the communication window, defined in subsection 5.7, the data has to be temporarily stored on-board before transmission to ground. With redundancies, onboard storage needs to handle at least 26.4 Gb of data for at least two days. The buffer has to be at least 10 Mb based on the expected one-minute data production and will be flushed regularly to limit the impact of Single Event Effects (SEEs). To mitigate the radiation effects, regular reboots of the systems and system redundancies are used.

5.4. Power

A power budget, found in Table 7, has been devised and power requirements have been defined.

5.4.1. Requirements

Considering the payload and essential onboard instruments, the design of the spacecraft necessitates a minimum continuous power output of 564 W. To ensure reliable functionality, the spacecraft will primarily rely on solar panels as its main power source, while also incorporating batteries to sustain a 2-hour operation in safe mode.

5.4.2. Solar Panels

To meet the power demands, the calculated solar panel area required is 6.49 m^2. The total power output of 2127 cells reaches a maximum of 1814 W. This value has been adjusted to account for various factors such as degradation of solar panels from radiation, maximum power point tracking (MPPT) efficiency of 98%, battery charge regulator (BCR)

Table 7
Power budget

LOAD	MAXIMUM POWER
OBDH	10.00 W
AODCS	80.00 W
EPS	90.00 W
COM	70.00 W
Thermal	80.00 W
Telescope	86.40 W
Margin	20 %
Total power	563.62 W

Table 8
Thermal requirements

COMPONENT	RANGE
Battery	283 K to 303 K
Fuel	288 K to 313 K
NIR detector	(120 ± 2) K
UV detector	293 K to 303 K
UV optical mirror	283 K $\pm$ 1 % rms

efficiency of 90%, and cell loss at maximum temperature. Additionally, a reduction in the effective active surface has been considered to account for variations in solar incidence during science operations. Specifically, the panels need to generate 464 W when tilted at an incidence angle of 75°.

5.4.3. Batteries
For a safe mode operation lasting 2 h, a 1000 Wh battery composed of 68 Li-Ion cells was deemed necessary. The calculations took into account a depth of discharge of 39.6%, ensuring an optimal balance between energy utilisation and battery lifespan.

5.5. Thermal
5.5.1. Requirements
To ensure the spacecraft's consistent performance, thermal constraints were calculated for each device that requires thermal control. The results are presented in the thermal requirements (Table 8), outlining specific thermal ranges for optimal functioning of the spacecraft's components.

5.5.2. Design
The spacecraft's thermal control system is designed for efficiency and simplicity. It features aluminium radiators for heat dissipation, inspired by the successful Hubble radiators used for IR detectors. The radiators are strategically placed on the spectrometer area, while a heater maintains the battery's optimal temperature. This design ensures consistent performance and thermal regulation for all the critical components.

Table 9
Mass Budget Summary

Subsystem	Planned (kg)	Contingency (% per kg)	Combined (kg)
OBDH	7.0	1.4	8.4
Thermal	20.0	4.0	
EPS	95.0	19.0	114.0
AODCS	130.1	26.0	156.2
COM	20.0	7.0	42.0
Structure	190.0	38.0	228.0
Payloads	286.3	57.3	343.6
Total Dry			**916.1**
Fuel			164.1
Wires		20.0	183.0
Margin		20.0	253.0
Total Wet			**1516.1**

5.6. Structure
During the structure design mission phase budget of the spacecraft, the mass has been calculated. It is provided in the mass budget summary Table 9.

5.6.1. Design
The spacecraft's structure is designed using Aluminum 7075, a lightweight and sturdy material. The choice of this material helps to keep the overall weight of the spacecraft low while ensuring structural strength during the mission Overall spacecraft structure can be seen in the Figure 10

5.6.2. Launcher
The spacecraft has been created to seamlessly integrate into the payload bay of the Ariane 62 launcher. During the structure design phase, resilience against vibration was considered. Moreover, the spacecraft structure was checked to be compatible with payload satellite adapters, further ensuring readiness for a successful mission.

5.7. Telecommunication
The spacecraft has to be able to facilitate two-way communications with ESA ground stations. To accomplish this, the 35 m ESA Deep Space Antennas (DSA) will constitute the ground segment while the spacecraft will host a 1 m^2 phased array similar to GAIA. The choice of a phased array over a traditional antenna disc eliminates the need for attitude changes between observation and telecommunication modes. Specifically, the spacecraft will use the X-band with a bandwidth of 10 MHz. Using a data rate of 8 Mbps in addition to the expected scientific data production of 13.2 Gb/day the nominal transfer window will be <30 min/day. Extended information about the link budget can be found in Table 10.

5.8. Operational Modes
The spacecraft will possess several operational modes, defining the active instruments and procedures. A short description of each mode is found in Table 11, and a detailed

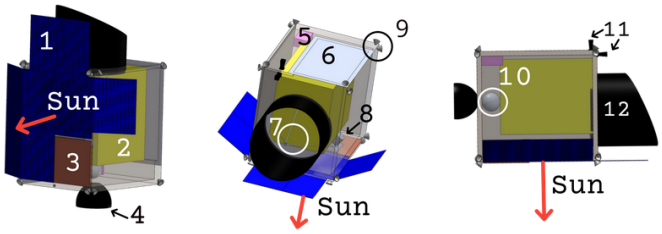

Figure 10: Spacecraft structure: 1 - solar panels, 2 - spectrometer, 3 - phased array antenna, 4 - orbital thruster, 5 - COM module, 6 - radiator, 7 - aperture, 8 - reaction wheels, 9 - RCS thrusters (x20), 10 - fuel tank, 11 - star tracker, 12 - baffle.

Table 10
A table of the link budget based on the spacecraft phased array and 35 m ESA DSAs.

	UPLINK	DOWNLINK
Frequency	**8.4 GHz**	**7.75 GHz**
EIRP	110.3 dB	33.3 dB
Pointing accuracy	0.15 deg	0.1 deg
Transmission loss	-236.5 dB	-235.8 dB
Receiver G/T	2.5 dB	51.7 dB
Data rate	**70 kbps**	**8 Mbps**
Final E_b/E_n	**3.3 dB**	**8.7 dB**

Table 11
Table and description of the different operational modes of the spacecraft.

MODE	DESCRIPTION
Safe	Troubleshooting
Commissioning	Instruments testing and health check
Orbital Maintenance	Making the L2 orbit stable
Course Pointing	Course pointing for target acquisition
Science	Fine pointing to target and scientific measurements
Telecommunication	Transmitting data to and from Earth

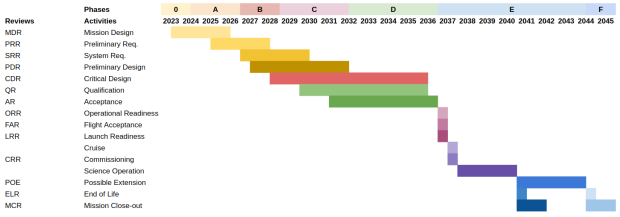

Figure 11: A Gantt chart over the estimated timeline of the mission.

Table 12
Table of the TRL of the spacecraft components.

PAYLOAD	TRL	SYSTEM	TRL
Telescope	4	Reaction wheels	9
Other optics	5	Thrusters	8
UV instrument	5	Star trackers	9
NIR instrument	5	Sun sensors	9
VIS instrument	5	Propulsion	8

Table 13
A table of the most important identified risks.

RISK	INDEX
Instrument damage	B4
Proxy disregard	C4
Mission Delay	D2

description of their estimated power consumption can be found in Table 7.

6. Programmatics

6.1. Timeline

The mission will aim for a launch in 2037 and will operate until the end of 2040 with a possible extension into 2044. A detailed Gantt chart is found in Figure 11.

6.2. Feasibility

For the mission to be viable, it has to be feasible from a technological and risk management perspective. The Technological Readiness Levels (TRLs) of the spacecraft components can be found in Table 12. The components with a TRL of 4-5 will need extensive functional verification in laboratories, thus extending the timeline in Figure 11 and the mission costs. Fortunately, the system components in Table 12 can be used off-shelf.

There are several identified risks with the mission. The most vital of these can be found in Table 13. The first risk includes mechanical damage, production deficits, and instrument contamination. To mitigate MS.01, vibrational testing, component monitoring, cleanrooms, and physical modeling will be used. The second risk describes the loss of scientific data due to ignoring certain atmospheric or magnetospheric proxies. This is mitigated by having redundancies in observed proxies in different spectral ranges. The final risk describes the risk of a mission delay due to component TRLs of 4-6. This can be mitigated through early testing of the telescope and the related optical and instrumental systems.

Table 14
Spacecraft costs

SPACECRAFT SEGMENT	COST [M€]
Telescope	150
UV, NIR and VIS instrument	80 + 50 + 30
Bus	150
Development/AIT	120
Data analysis (8 scientists for 3 years)	23
Launcher	75
Total cost 20% margin	813.6

6.3. Costs

As shown in Table 14 and according to ESA classification, the mission fits the criteria of an L-mission, reaching 730 million euros.

6.4. Outreach

In accordance with ESA's *Agenda 2025*, outreach strategy focuses on European education and talent acquisition, targeting the scientific community through publications, conferences, observation proposals, and open mission meetings for students. The general public will be engaged via social media, podcasts, an observational findings app, educational resources, and interactive exhibitions.

7. Acknowledgements

The Red Team wishes to express its utmost gratitude to the tutors, Elise and Ricardo, whose patience and understanding kept us on duty. To the lecturers, your participation brought us valuable professional and personal teaching. Special thanks to Tibor Agocs for his unflinching support. To the organizing team, thank you for having us in your care. See you all starside.

References

[1] 7 2023. [Online]. Available: https://exoplanets.nasa.gov

[2] P. J. Sebastian *et al.*, "A panchromatic view of brown dwarf aurorae," *The Astrophysical Journal*, September 2017.

[3] J. Saur *et al.*, "Brown dwarfs as ideal candidates for detecting uv aurora outside the solar system: Hubble space telescope observations of 2mass j1237+6526," *Astronomy & Astrophysics*, November 2021.

[4] D. A. Ruíz-Rodríguez *et al.*, "Discovery of a brown dwarf with quasi-spherical mass loss," *The Astrophysical Journal,*, October 2022.

[5] G. M. Szabó *et al.*, "The sub-jupiter/neptune desert of exoplanets: parameter dependent boundaries and implications on planet formation," *Monthly Notices of the Royal Astronomical Society: Letters*, May 2019.

[6] M. Zhang *et al.*, "Detection of atmospheric escape from four young mini-neptunes," *The Astronomical Journal*, January 2023.

[7] J. Venturini *et al.*, "The nature of the radius valley-hints from formation and evolution models," *Astronomy & Astrophysics*, vol. 643, p. L1, 2020.

[8] A. Gupta *et al.*, "Signatures of the core-powered mass-loss mechanism in the exoplanet population: dependence on stellar properties and observational predictions," *Monthly Notices of the Royal Astronomical Society*, vol. 493, no. 1, pp. 792–806, 2020.

[9] A. Izidoro *et al.*, "The exoplanet radius valley from gas-driven planet migration and breaking of resonant chains," *The Astrophysical Journal Letters*, vol. 939, no. 2, p. L19, 2022.

[10] H. Gunell *et al.*, "Why an intrinsic magnetic field does not protect a planet against atmospheric escape," *Astronomy & Astrophysics*, vol. 614, p. L3, 2018.

[11] A. Yuki *et al.*, "Atmospheric escape by magnetically driven wind from gaseous planets. ii. effects of magnetic diffusion," *The Astrophysical Journal*, August 2015.

[12] K. Fan *et al.*, "Deflection of global ion flow by the martian crustal magnetic fields," *The Astrophysical Journal Letters*, August 2020.

[13] I. Dandouras, "Ion outflow and escape in the terrestrial magnetosphere: Cluster advances," *Journal of Geophysical Research: Space Physics*, vol. 126, no. 10, p. e2021JA029753, 2021.

[14] J. E. Owen *et al.*, "The fundamentals of Lyman-alpha exoplanet transits," *Monthly Notices of the Royal Astronomical Society*, vol. 518, no. 3, pp. 4357–4371, 11 2022. [Online]. Available: https://doi.org/10.1093/mnras/stac3414

[15] D. Ehrenreich *et al.*, "A giant comet-like cloud of hydrogen escaping the warm neptune-mass exoplanet gj 436b," *Nature*, vol. 522, pp. 459–61, 06 2015.

[16] L. A. G. D. SANTOS, "Atmospheric escape in exoplanets: A journey from gas giants to earth twins," 2021.

[17] A. Oklopčić *et al.*, "A new window into escaping exoplanet atmospheres: 10830 Å line of helium," *The Astrophysical Journal Letters*, vol. 855, no. 1, p. L11, mar 2018. [Online]. Available: https://dx.doi.org/10.3847/2041-8213/aaada9

[18] M. Zhang *et al.*, "Detection of atmospheric escape from four young mini-neptunes," *The Astronomical Journal*, vol. 165, no. 2, p. 62, jan 2023. [Online]. Available: https://dx.doi.org/10.3847/1538-3881/aca75b

[19] J. Llama *et al.*, "The shocking transit of wasp-12b: modelling the observed early ingress in the near-ultraviolet," *Monthly Notices of the Royal Astronomical Society: Letters*, vol. 416, no. 1, pp. L41–L44, 2011.

[20] K. Herbst *et al.*, "Astrospheres of planet-hosting cool stars and beyond when modeling meets observations," *Space Science Reviews*, vol. 218, no. 4, p. 29, 2022.

[21] J. Seidel *et al.*, "Wind of change: retrieving exoplanet atmospheric winds from high-resolution spectroscopy," *Astronomy & Astrophysics*, vol. 633, p. A86, 2020.

[22] M. Montalto *et al.*, "The all-sky plato input catalogue," *A&A*, vol. 653, p. A98, 2021. [Online]. Available: https://doi.org/10.1051/0004-6361/202140717

[23] European Space Agency. Ariel payload. Last access: 19.07.2023. [Online]. Available: https://sci.esa.int/web/ariel/-/59801-payload

[24] L. Ben-Jaffel *et al.*, "Exoplanet hd 209458b: Inflated hydrogen atmosphere but no sign of evaporation," *The Astrophysical Journal*, vol. 671, no. 1, p. L61, 2007.

[25] L. BenJaffel *et al.*, "Signatures of strong magnetization and a metal-poor atmosphere for a neptune-sized exoplanet," *Nature Astronomy*, vol. 6, no. 1, pp. 141–153, 2022.